The glutamate/aspartate transporter EAAT1 is crucial for T-cell acute lymphoblastic leukemia proliferation and survival

Vesna S. Stanulović,[1] Shorog Al Omair,[1] Michelle A.C. Reed,[1] Jennie Roberts,[1] Sandeep Potluri,[1] Taylor Fulton-Ward,[2] Nancy Gudgeon,[2] Emma L. Bishop,[2] Juliette Roels,[3] Tracey A. Perry,[1] Sovan Sarkar,[1] Guy Pratt,[1,4] Tom Taghon,[3] Sarah Dimeloe,[2] Ulrich L. Günther,[1] Christian Ludwig[5] and Maarten Hoogenkamp[1]

[1]Institute of Cancer and Genomic Sciences, University of Birmingham, Birmingham, UK; [2]Institute of Immunology and Immunotherapy, University of Birmingham, Birmingham, UK; [3]Department of Diagnostic Sciences, Ghent University, Ghent, Belgium; [4]Center for Clinical Hematology, Queen Elizabeth Hospital Birmingham, Birmingham, UK and [5]Institute of Metabolism and Systems Research, University of Birmingham, Birmingham, UK

Correspondence: M. Hoogenkamp
m.hoogenkamp@bham.ac.uk

Received: May 3, 2023.
Accepted: May 20, 2024.
Early view: May 30, 2024.

https://doi.org/10.3324/haematol.2023.283471

Abstract

T-cell acute lymphoblastic leukemia (T-ALL) is a cancer of the immune system. Approximately 20% of pediatric and 50% of adult T-ALL patients have refractory disease or relapse and die from the disease. To improve patient outcome new therapeutics are needed. With the aim to identify new therapeutic targets, we combined the analysis of T-ALL gene expression and metabolism to identify the metabolic adaptations that T-ALL cells exhibit. We found that glutamine uptake is essential for T-ALL proliferation. Isotope tracing experiments showed that glutamine fuels aspartate synthesis through the tricarboxylic acid cycle and that glutamine and glutamine-derived aspartate together supply three nitrogen atoms in purines and all but one atom in pyrimidine rings. We show that the glutamate-aspartate transporter EAAT1 (*SLC1A3*), which is normally expressed in the central nervous system, is crucial for glutamine conversion to aspartate and nucleotides and that T-ALL cell proliferation depends on EAAT1 function. Through this work, we identify EAAT1 as a novel therapeutic target for T-ALL treatment.

Introduction

T-cell acute lymphoblastic leukemia (T-ALL) are hematological malignancies of the T-cell lineage. Subtypes are grouped based on immunophenotype, or more recently, gene expression profiling that correlates with the underlying genomic aberrations.[1,2] T-ALL occurs both in adults and children and, despite improved treatment outcome in the last decades, up to 20% of pediatric and 50% of adult T-ALL patients have refractory disease or relapse.[3-6] Alternative treatment options are not available for these patients and, therefore, novel therapeutic targets are needed.

For a cancer to proliferate, cells need to increase their size and replicate their DNA, which requires large quantities of proteins, lipids and nucleotides, as well as energy. Cell proliferation and survival require metabolic adaptations, involving glycolysis, glutaminolysis and the PI3K-AKT-mTOR pathway.[7-12] Differences in the reliance on glutamine and glutaminolysis between B-ALL and T-ALL have been observed.[13,14] Metabolic adaptations and mutations, such as Notch1 mutations, have been correlated with glutamine dependency in T-ALL.[15-17] The compilation of metabolic changes results in distinct metabolic phenotypes and determination of the rate-limiting steps that support the oncogenic metabolic adaptations can lead to the identification of novel therapeutic targets.

With the aim to identify common oncogenic adaptations, we investigated T-ALL metabolism, using cell lines, representing different stages of T-cell development, and primary patient samples. We found that T-ALL cells take up glutamine and use it to generate aspartate. Normally, glutamine and aspartate are used as substrates for *de novo* nucleotide production but in T-ALL, glutamine alone provides all of the nitrogen atoms and all but one carbon atom in the pyrimidine ring, and three of the four nitrogens in purines. Furthermore, we determined that T-ALL cells express the glutamate-aspartate antiporter EAAT1 (encoded by *SLC1A3*), which is present in 95% of T-ALL patients.[2] In the healthy adult body, EAAT1 is only present in the neurons and glia of the central nervous system (CNS) where it removes cytotoxic glutamate from the glutamatergic synapses in exchange for aspartate.[18,19] In T-ALL,

EAAT1 is required for glutamate import into mitochondria in exchange for glutamine-derived aspartate which is then used as a substrate for nucleotide production in the cytoplasm. We show that T-ALL survival depends on glutamine uptake and EAAT1 function, which validates EAAT1 as a therapeutic target for treating T-ALL.

Methods

Detailed information is available in the *Online Supplementary Appendix*.

Cell culture

T-ALL cell lines were grown in RPMI-1640 medium. For labeling experiments, glutamine-free RPMI was supplemented with 2 mM [1,5-^{15}N]-L-glutamine or [3-^{13}C]-L-glutamine (Merck).
In vitro differentiation of human T-cell progenitors was performed using mononuclear cells isolated from cord blood; Human Biomaterials Resource Center approval 15/NW/0079. CD34$^+$ cells were co-cultured on OP9-DL4 cells in αMEM medium with hFLT3L and hIL7.
CD4$^+$/CD8$^+$ T cells were isolated from leukocyte cones (UoB STEM Ethics ERN_17-1743) and left unstimulated or stimulated for 48 hours (h).

Expression analysis

RNA isolation and cDNA synthesis was performed as previously described.[20] RNA-sequencing (RNAseq) libraries were prepared and indexed using the TruSeq Stranded mRNA Sample Preparation Kit LH. Libraries were pooled and sequenced as 100-nucelotide paired-end on Illumina HiSeq2500 sequencer.

Western blot analysis

Cell extracts were prepared in RIPA buffer. Proteins were separated on acrylamide gels, transferred to nitrocellulose membranes and stained with PonceauS to confirm equal loading, prior to overnight (o/n) incubation with primary antibody. Secondary antibodies were visualized using an Odyssey CLx Imager.

Immunofluorescent staining

Cells were fixed with formaldehyde, washed with phosphate-buffered saline (PBS)/0.05%Tween/2% fetal calf serum, followed by o/n incubation with primary antibody. Cells were washed and incubated with secondary antibody conjugated to Alexa dyes before being deposited onto glass slides using a Cytospin III centrifuge. MitoTracker Red CMXRos was used for mitochondria staining.

SLC1A3 knockdown

SLC1A3 was cloned into MigR1 in front of IRES-GFP.[21] Short hairpin (sh) sequences targeting *SLC1A3* were embedded into miR30 and cloned into pMSCVhygro.[22] The mouse fibroblast cell line PlatE was transfected using *Trans*IT-LT1 with MigRI-SLC1A3 and MSCVhyg_shSLC1A3, MSCVhyg_shGFP, or MSCVhyg_shFF3.[23,24] Functional shRNA was cloned into PiggyBac transposon doxycycline-inducible expression vector PB_tet-on_Apple_shGFP.[25] T-ALL cell lines were electroporated with pB_shSLC1A3 and p*CAGG-Pbase*,[26] expanded and selected with puromycin prior to doxycycline induction.

Patient samples

Patients' cells were from diagnostic samples from presentation cases, with ethical approval from the NHS National Research Ethics Committee (Reg: 10/H1206/58). Blast cells were isolated from mononuclear cells using anti-human CD34 (T-ALL_1 and _2) or CD7 (T-ALL_3) MACS microbeads. For T-ALL_2, CD34$^+$ cells were further sorted by fluorescence-activated cell sporting (FACS) for CD7$^+$, using anti-human CD7-FITC antibody.

Nuclear magnetic resonance spectroscopy

For intracellular measurements, polar cell extracts were resuspended in nuclear magnetic resonance (NMR) buffer and transferred to NMR tubes. Spectra were acquired using a Bruker 600 mHz spectrometer.
For uptake and release experiments, growth medium was collected and supplemented with 1 mM TMSP, 10% D_2O. Spectra were acquired using a Bruker 500 MHz spectrometer.
For live-cell real-time NMR spectroscopy, cells were resuspended at 10^6/mL growth media containing 0.1% low melting agarose, 1 mM TMSP, 10% D_2O. Spectra were acquired using a Bruker 500 MHz spectrometer.
NMR spectroscopy data was processed in Topspin, MetaboLab in MATLAB[27] and MetaboLabPy (https://pypi.org/project/qtmetabolabpy).

Mouse studies

Animal experiments were performed at the University of Birmingham Biomedical Services Unit under an animal project license (PP8841933) in accordance with UK legislation. Female NOD.Cg-Prkdc^{scid} Il2rg^{tm1Wjl}/SzJ (NSG) mice, aged 8-9 weeks at study commencement, were used. CCRF-CEM cells were transfected with pBshSLC1A3_2 or pBshGFP control vector and pCAGG-PBase. After selection, 3x10^5 cells/mouse were injected into the tail vein. When approximately 1% engraftment was observed, next day all animals were transferred to a diet supplemented with 0.625 g/kg doxycycline-hyclate.

Results

T-cell acute lymphoblastic leukemia metabolic phenotype

For our study, we chose four T-ALL cell lines that have different immunophenotypes, reflecting that the T cells are blocked at different stages of development. Their immunophenotype and corresponding EGIL classification are

indicated in *Online Supplementary Figure S1*.[28] In order to assess leukemic adaptation, we compared the gene expression of these cell lines to the gene expression of *in vitro* differentiated T-cell progenitors at the $CD7^+$ $CD5^-$ $CD1a^-$, the $CD7^+$ $CD5^+$ $CD1a^-$, and the $CD7^+$ $CD5^+$ $CD1a^+$ $CD3^-$ stage of differentiation. Analyses of the RNAseq data identified 2,072 significantly differentially expressed genes, grouped by hierarchical clustering into two clusters (Figure 1A; *Online Supplementary Table S1*). Genes suppressed in the T-ALL cells were grouped in cluster 1 (C1, 1,287 genes) while upregulated genes were in cluster 2 (C2, 786 genes). Gene functional annotation clustering analyses found 53 statistically significantly enriched functional clusters in C1 and 22 in C2 (*Online Supplementary Tables S2, S3*). Amongst the top ten highest enriched clusters for C1 were: glycyl-lysine isopeptide bond with SUMO2, RNA splicing, translation, DNA repair, DNA binding and localization to mitochondrion. For C2 genes encoding proteins containing BTB/POZ, LRR and PH protein domains, phospholipase C-activating G-protein-coupled receptor signaling, sequence-specific double stranded DNA-binding and extracellular matrix proteins were found (Figure 1B; *Online Supplementary Table S4*). The largest cluster was composed of 123 genes whose product has lysine that is crosslinked through the isopeptide bond with C-terminal glycine of SUMMO2 protein. Amongst the genes were transcription factors (FOXP1, ELK4, IKZF5, TCFL2, ZEB2) and chromatin modifiers (KMT2B, BRD7, CHD4, CHD9). The second largest (86 genes) was the group of mitchondrial proteins important for the mitochondrial respiratory chain complex I assembly (LYRM2, NDUFA2, NDUFB9 and TMEM186), regulation of mitochondrial membrane potential (PRELID1, SOD2 and ubiquitin B), ATP biosynthetic process (COX11, DGUOK and UQCC3) and TCA cycle (IDH3A, PDHB and SDHC).

We therefore investigated the metabolism of the TALL cell lines. Metabolite uptake was assessed by measuring metabolite levels in the media, 24 h after medium change, by NMR spectroscopy and comparing it to the levels present in the media alone. We identified 22 metabolites with significantly changing levels in at least one of the T-ALL cell lines and found that all four cell lines utilized lysine, glucose, phenylalanine and glutamine and released lactate, pyruvate, glutamate and pyroglutamate (Figure 2A).

In order to assess how uptake influences intracellular metabolite levels we compared the abundance of intracellular metabolites at the time of growth-media change (0 h) to that seen 8 h and 24 h later (Figure 2B). A similar response to media change in all four cell lines was found only for glutamate and myoinositol, whose intracellular concentration decreased upon media supplementation. Glutamate and myoinositol are important metabolites for every proliferating cell as they are used to fuel cell growth and proliferation. Myoinositol is used as a substrate for membrane synthesis while glutamate feeds into the TCA cycle hence, energy production. Observed glutamine uptake and glutamate utilization by T-ALL cell lines suggest that glutamine is used to support the cellular demand for glutamate (Figure 2A, B).

Glutamine is essential for T-cell acute lymphoblastic leukemia proliferation and survival

Next, we wanted to determine the importance of glutamine for T-ALL. We therefore tested the effect of glutamine withdrawal on cellular proliferation. Omitting glutamine from the growth medium, while maintaining all other nutrients, including 10% fetal bovine serum, reduced T-ALL cell numbers by 95% after 8 days of treatment, except for ARR where the proliferation decreased over the first 4 days, after which ARR resumed proliferation (Figure 2C). Another two cell lines, Molt-4 and Jurkat, were tested as well, which showed that Molt-4 was sensitive to glutamine withdrawal, whereas Jurkat showed growth kinetics similar to ARR (*Online Supplementary Figure S2A*). Glutamine dependency did not correlate with oncogenic subtype, differentiation stage or Notch mutation status (*Online Supplementary Figure S2B*).[29] Apoptosis assays of the cells grown in glutamine-free medium revealed that the T-ALL cell lines had an increased rate of apoptosis (*Online Supplementary Figure S3A*), while cell cycle analysis showed a reduction of cells in S-phase (*Online Supplementary Figure S3B*), indicating that glutamine is important for T-ALL cell proliferation and survival.

Glutamine fuels aspartate and nucleotide biosynthesis

Glutamine has several significant roles in metabolic processes, such as fueling the tricarboxylic acid (TCA) cycle through glutaminolysis, acting as a nitrogen donor in transamination and transamidation reactions, and *de novo* nucleotide synthesis. Aspartate, glycine, glutamate and alanine can be derived from glutamine, and glutamine, glycine and aspartate are used as substrates for nucleotide synthesis. In order to assess the glutamine contribution to T-ALL metabolic processes we performed tracer experiments using [2,5-^{15}N]glutamine and [3-^{13}C]glutamine. When cells were grown in the presence of [2,5-^{15}N]glutamine, in addition to the expected ^{15}N-labeled glutamate *(data not shown*), we observed ^{15}N incorporation into the amino group of aspartate and alanine within 8 h of treatment for all four cell lines (Figure 3A; *Online Supplementary Figure S4A*). For aspartate, at 0 h, a doublet was seen due to coupling to the Hα. At later time points there was increased spectral complexity due to weak coupling of Hβs to ^{15}N. The resulting spectrum was a weighted average of a doublet of doublets (from ^{15}N-labeled aspartate) and a simple doublet (unlabeled aspartate) (Figure 3A). This demonstrates that glutamine-derived ^{15}N was incorporated into aspartate and alanine by transamination of oxaloacetate and pyruvate, respectively.

In order to assess the contribution of glutamine to nucleotide biosynthesis, we first acquired 2D-^{1}H,^{15}N heteronu-

clear single quantum coherence (HSQC) NMR spectra of ^{15}N uniformly labeled ATP, GTP and UTP standards, where we observed five ^{1}H-^{15}N interactions for [U-^{15}N]ATP (a-d), three for [U-^{15}N]GTP (a-c) and three for [U-^{15}N]UTP (a-c) (Figure 3B). Spectra acquired from [2,5-^{15}N]glutamine-labeled T-ALL cells showed ^{15}N incorporation into nucleotides at the 1, 3 and 9 positions, the 3 and 9 positions and the 1 and 3 positions for adenine, guanine and uracil respectively (Figure 3B). As expected, transamidation using ^{15}N-glutamine resulted in label incorporation at N-3 and N-9 in purines and the N-3 in pyrimidines. Additional label incorporation at N-1 in purines and N-3 in pyrimidines is sourced from glutamine-derived ^{15}N-aspartate and shows that glutamine ultimately supplies all but one nitrogen in purine and both nitrogens in the pyrimidine ring.

We demonstrated that glutamine transamination of oxalo-

A

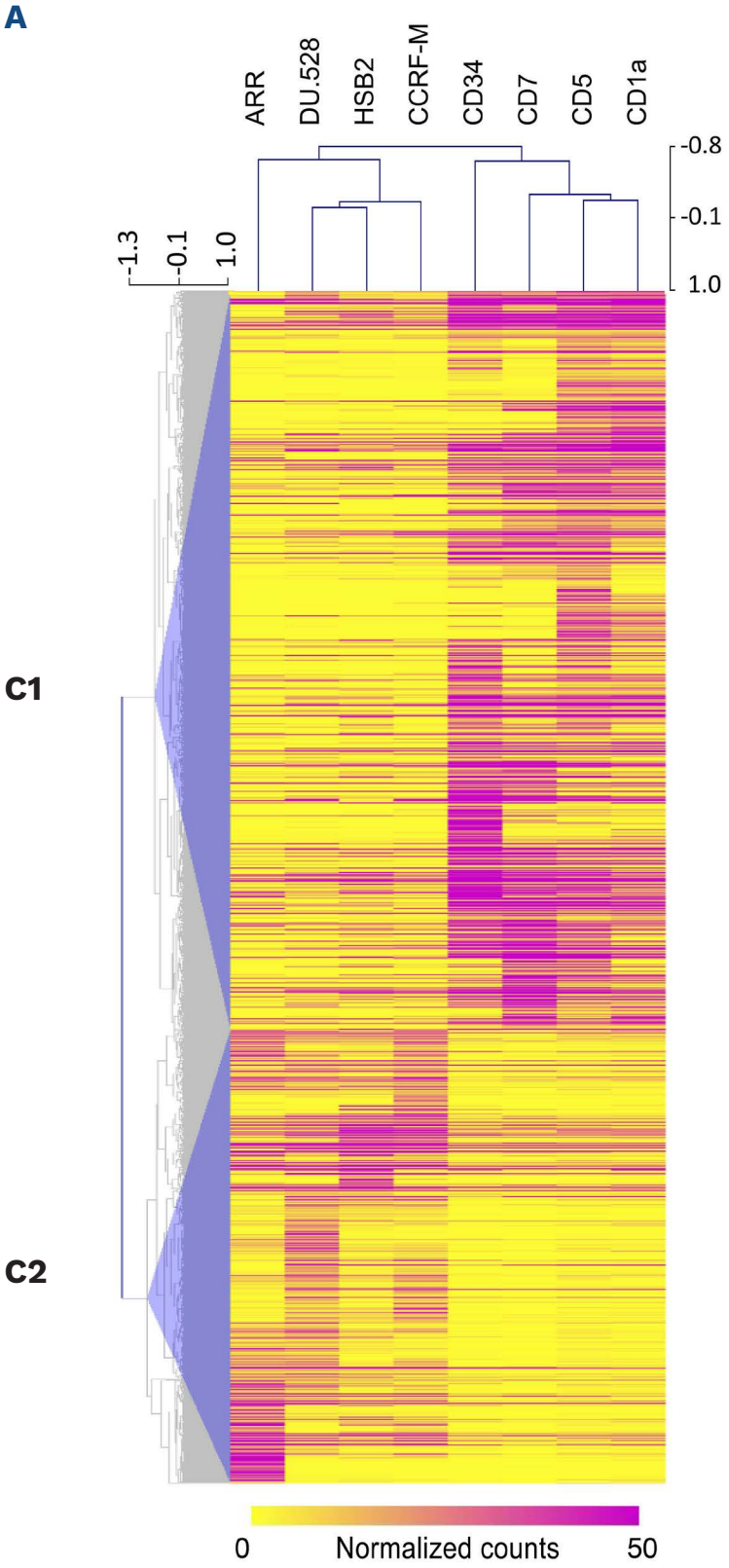

B

Functional Annotation Clustering (2,072 genes)			
Cluster 1 (1,285 Genes)			
Enrichment Score	Term	*P*	Gene Count
17.04	Glycyl lysine isopeptide (Lys-Gly) (interchain with G-Cter in SUMO2)	5.6E-20	123
5.06	RRM (RNA-binding domain)	1.3E-07	30
4.72	Cytoplasmic translation	5.4E-07	17
4.54	RNA splicing	3.5E-07	27
3.99	DNA repair	3.9E-05	35
2.94	Chaperone	1.2E-04	25
2.78	Mitochondrion	1.6E-04	84
1.80	Cytosolic small ribosomal subunit	2.3E-03	8
1.78	Damaged DNA binding	6.8E-03	9
1.65	Protein biosynthesis	1.3E-02	15

Cluster 2 (786 Genes)			
Enrichment Score	Term	*P*	Gene Count
3.74	Nuclear testis protein, N-terminal	6.2E-05	4
3.00	Proteins containing BTB domain	4.6E-04	9
1.95	LRR 5 (Leucine-rich repeat 5) domain	1.8E-03	10
1.93	Phospholipase C-activating G-protein coupled receptor signaling pathway	3.8E-04	7
1.22	FBG (Fibrinogen)	2.8E-02	3
1.19	Sequence-specific double-stranded DNA binding	4.7E-03	14
1.17	Melanogenesis	2.1E-02	5
0.95	Palmitate	3.5E-02	9
0.91	Extracellular matrix	1.4E-02	8
0.90	PH (Pleckstrin homology domain)	7.2E-02	7

Figure 1. Differential gene expression and gene ontology analysis for T-cell acute lymphoblastic leukemia cell lines. (A) Heat map showing hierarchical clustering of the significantly differentially expressed genes between the T-cell acute lymphoblastic leukemia (T-ALL) cell lines (ARR, DU.528, HSB2 and CCRF-CEM), healthy CD34^{+} cells isolated from umbilical cord blood and T-cell progenitors (CD7^{+} CD5^{-} CD1a^{-}, CD7^{+} CD5^{+} CD1a^{-}, and CD7^{+} CD5^{+} CD1a^{+} CD3^{-}) derived from the differentiation of CD34^{+} progenitors on OP9-DL4 stromal cells. RNA-sequencing (RNAseq) gene expression data are gene-normalized counts clustered based on Pearson correlation with average linkage clustering. Two clusters are marked by blue triangles and numbered 1 and 2. Scale bar represents gene normalized counts from 0 to 50. (B) Gene functional annotation clustering for clusters 1 and 2. Terms are ordered based on their enrichment score. Modified Fisher extract *P* value and gene count are shown. Further details are available in *Online Supplementary Table S4*.

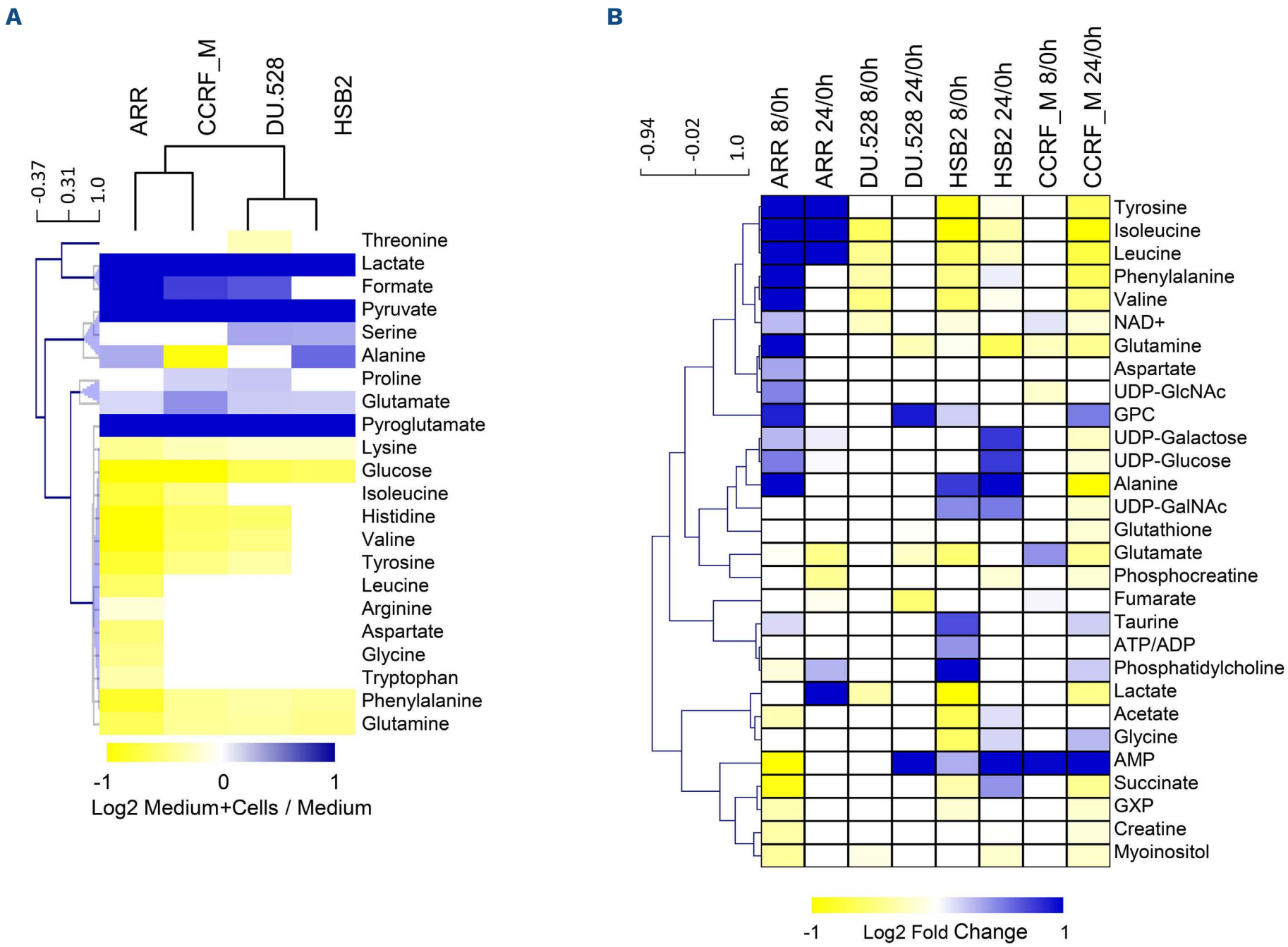

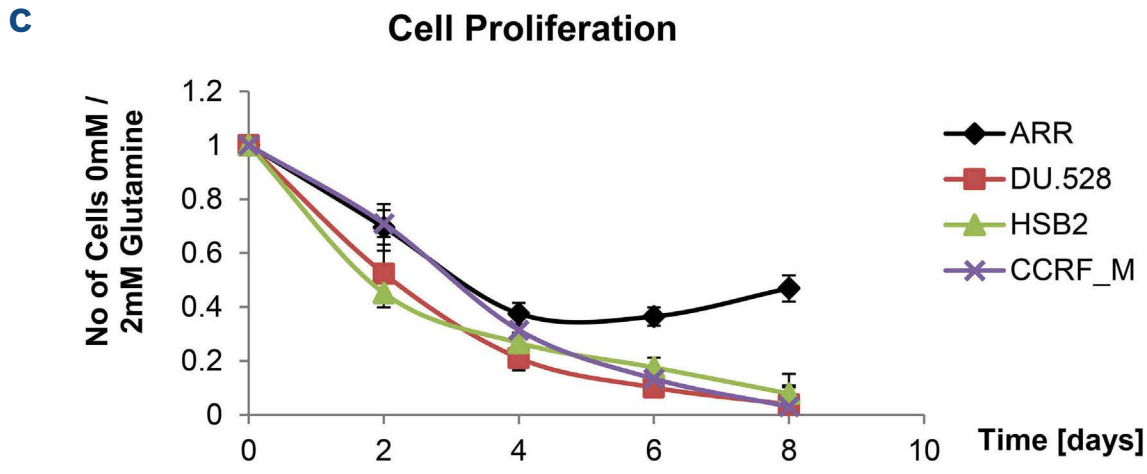

Figure 2. Metabolite levels in T-cell acute lymphoblastic leukemia cells are dynamic. (A) Heat map showing hierarchical clustering of the growth medium metabolites after 24 hours (h). Data are the average of 4 independent experiments ± standard deviation (SD). Scale bar represents log2 relative metabolite concentration. Metabolites with significantly different levels are shown. (B) Abundance of intracellular metabolites at 8 h or 24 h, relative to the time of medium change (0 h). Fold change was presented only for metabolites with significantly different relative levels with $P<0.05$. GPC: L-α glycerylphosphorylcholine; GalNAc: acetylgalactosamine; GlcNAc: N-acetylglucosamine. (C) Glutamine deprivation inhibits T-cell acute lymphoblastic leukemia (T-ALL) cell proliferation. T-ALL cell lines were cultured in medium with 10% fetal bovine serum, with or without 2 mM GlutaMax. Four independent cell cultures were assayed per cell line and each point represents the mean ± SD. Statistically significant differences were found when ARR was compared to any of the other cell lines at day 6 and 8 ($P<0.05$).

acetate gives rise to aspartate. It is possible that glutamine supplies oxaloacetate, through glutaminolysis, which would consequently mean that aspartate is completely derived from glutamine. We used [3-^{13}C]glutamine in labeling experiments to test this. Within the TCA cycle, [3-^{13}C]glutamine is converted to [2-^{13}C]fumarate, a symmetrical molecule which is hydrated equally to [2-^{13}C]malate and [3-^{13}C]malate, and further to [2-^{13}C] or [3-^{13}C]oxaloacetate and aspartate (SI3). Acquired 2D-^{1}H,^{13}C HSQC NMR spectra revealed ^{13}C incorporation in fumarate, malate, oxaloacetate and aspartate (Figure 4A; *Online Supplementary Figure S4B*). Resonances for ^{1}H-^{13}C moieties were derived from both [2-^{13}C] and [3-^{13}C] labeling, as shown for aspartate and malate (a and b respectively; Figure 4A; *Online Supplementary Figure S2B*). Quantification of the signals from the labeled samples, relative to the naturally occurring ^{13}C

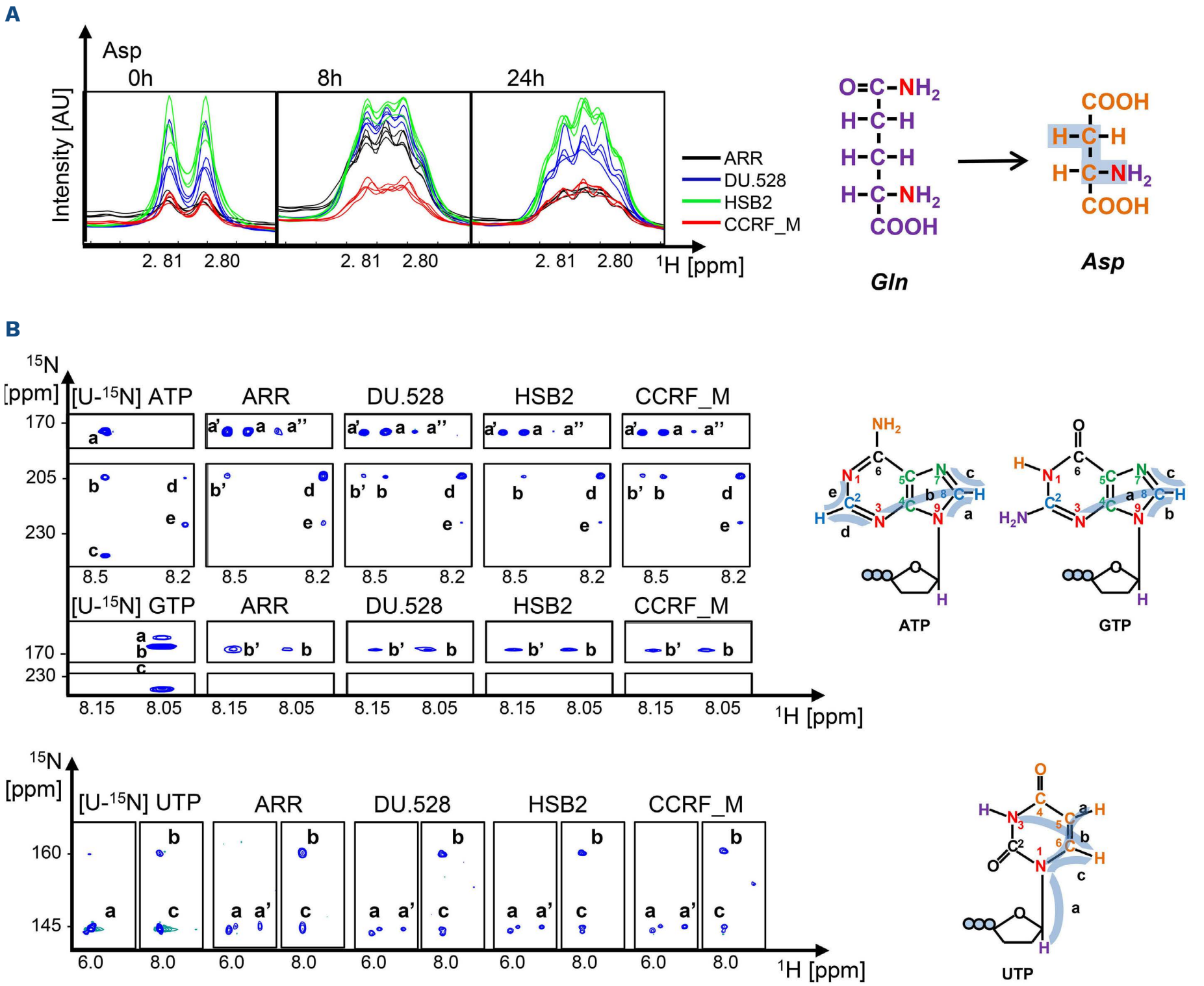

Figure 3. T-cell acute lymphoblastic leukemia cells utilize glutamine-derived nitrogen for *de novo* nucleotide synthesis. Metabolite tracing experiments using T-cell acute lymphoblastic leukemia (T-ALL) cell lines that were grown in the presence of 2 mM [2,5-^{15}N]glutamine. (A) Overlay of 1D 1H-nuclear magnetic resonance (NMR) spectra showing the Hβ-aspartate resonance after 0, 8 and 24 hours (h) and schematic representations of [2,5-^{15}N]glutamine and the observed [2-^{15}N]aspartate. ^{15}N are in red and shading indicates the observed ^{3}J scalar couplings between the aspartate Hβ and glutamine-derived ^{15}N. The X-axis shows the chemical shift relative to TMSP in ppm and the Y-axis indicates TSA scaled intensity. (B) Resonances observed in ^{1}H-^{15}N-HSQC for [U-^{15}N]ATP, [U-^{15}N]GTP, [U-^{15}N]UTP standards and for T-ALL cells extracts grown for 24 h in the presence of [2,5-^{15}N]glutamine. Resonances are marked by letters a-e. Schematics show ATP, GTP and UTP with color-coded atoms based on the substrate of their origin (glutamine-purple, aspartate-orange, glycine-green, carbonate-black and ^{15}N-red). Blue shaded lines indicate observed couplings annotated a-e. Asp: aspartate; Gln: glutamine; ATP: adenosine triphosphate; GTP: guanosine-5'-triphosphate; UTP: uridine-5′-triphosphate.

in the control samples, showed that within 24 h, 40-70% of aspartate was [2-^{13}C] or [3-^{13}C]aspartate (Figure 4B). These findings confirm that two molecules of glutamine give rise to a single aspartate molecule; first glutamine supplies the backbone via the TCA cycle, while the second is used for transamination. These metabolic conversions occurred in all four tested T-ALL cell lines even though we observed that ARR also uptake aspartate from the media (Figure 2A), suggesting that the aspartate uptake in ARR is not sufficient to support its demand.

A further implication of these findings was that carbons derived from glutamine would, via aspartate, get incorporated into pyrimidines, giving rise to [5-^{13}C] or [6-^{13}C] uridine. This was indeed observed in 2D-^{1}H,^{13}C HSQC NMR spectra (peaks a and b; Figure 4A, B), showing that the carbon at position 4 also originates from glutamine via aspartate. Together, our results show that glutamine serves as a source for all but one of the atoms in the pyrimidine ring.

Additionally, examination of the ^{13}C incorporation in other

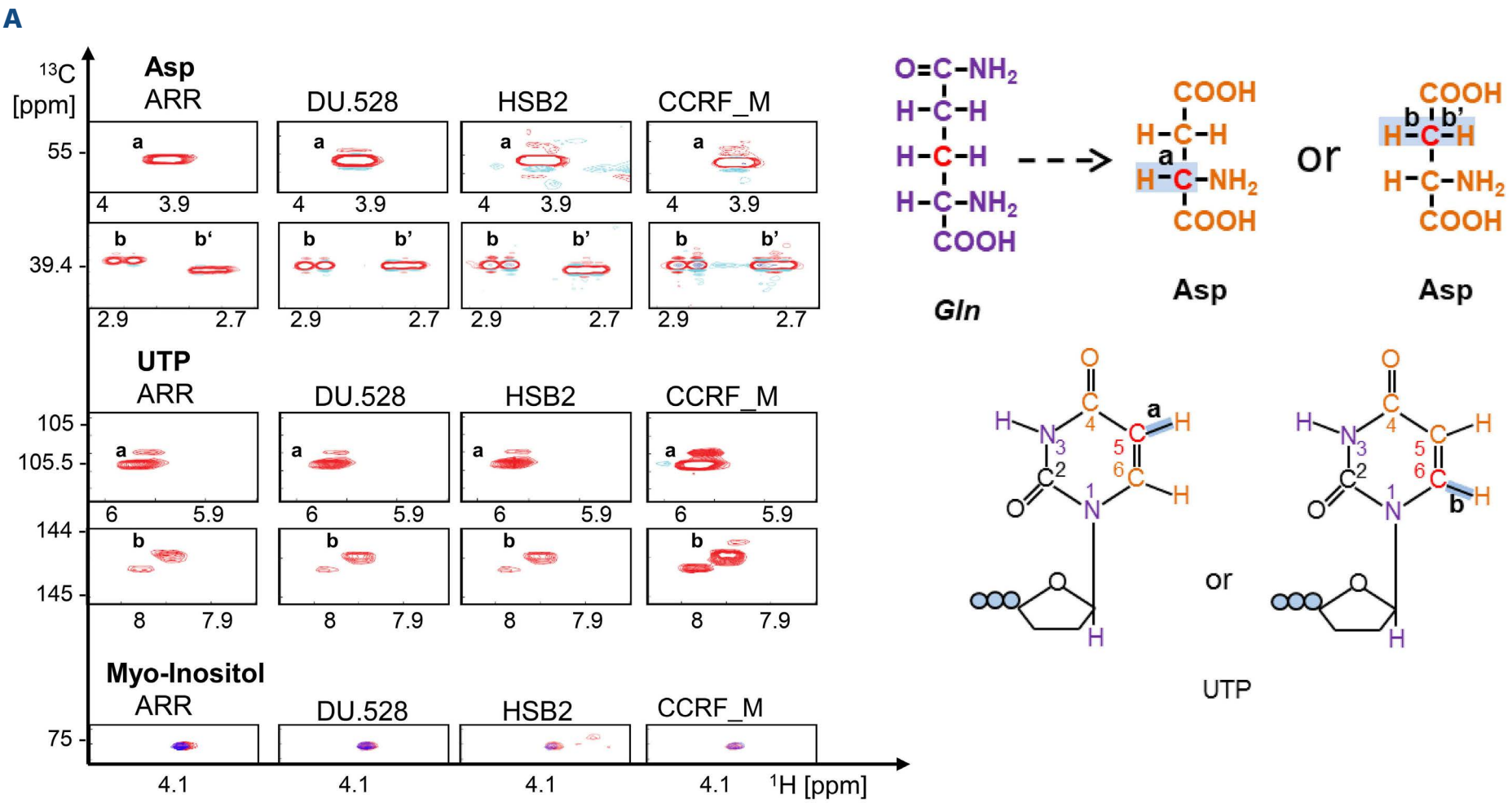

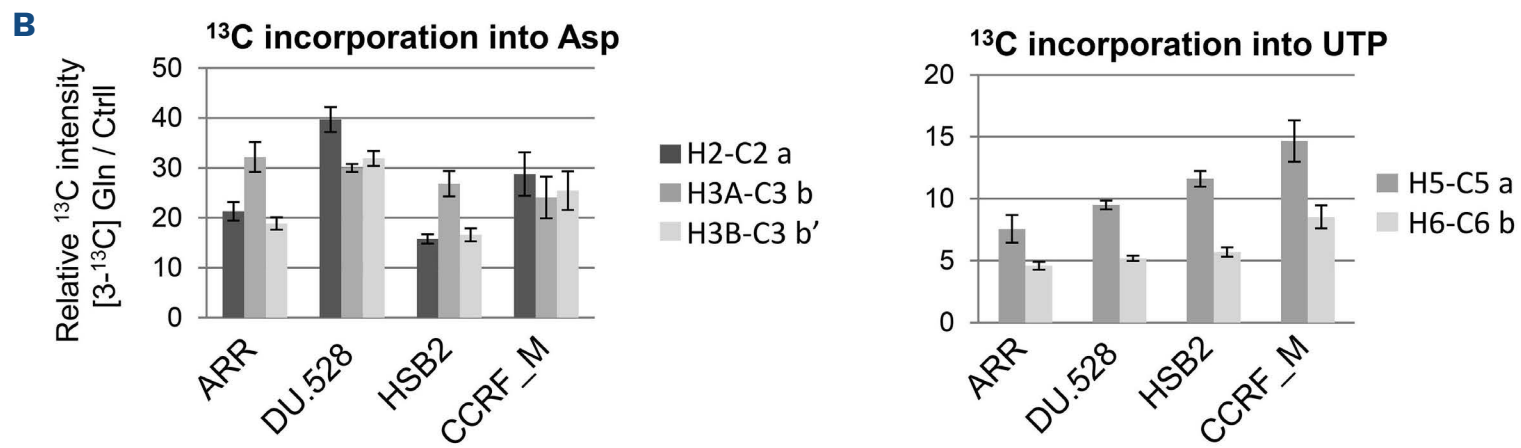

Figure 4. T-cell acute lymphoblastic leukemia cells utilize glutamine-derived carbon for *de novo* nucleotide synthesis. (A) Resonances observed in ^{1}H-^{13}C-HSQC for T-cell acute lymphoblastic leukemia (T-ALL) cells grown for 24 hours (h) in the presence of [3-^{13}C]glutamine. Resonances are marked by letters a-e. Schematics on the right show glutamine, aspartate and uridine-5'-triphosphate (UTP) with color-coded atoms based on the substrate of their origin. Blue shaded lines indicate observed couplings annotated a-e. (B) Quantification of glutamine (Gln)-derived aspartate (Asp) and uridine diphosphate (UDP). Bar graphs show ^{13}C signal intensity acquired from the cells grown in the presence of [3-^{13}C]glutamine for 24 h, relative to the signal acquired from the naturally occurring ^{13}C observed in the extracts from cells grown without the label. Each bar represents one of the interactions shown in the schematics in (A). Data are the average of at least 3 independent experimental measurements ± standard deviation.

detectable metabolites found a significant label accumulation into proline, as would be expected since glutamate is used as a substrate for proline synthesis (*Online Supplementary Figure S4C*).

Patient-derived T-cell acute lymphoblastic leukemia and T-cell acute lymphoblastic leukemia cell lines have similar metabolic uptake

In order to determine if glutamine is not only used by patient-derived cell lines, but also by primary T-ALL patient isolates, we measured live-cell real-time metabolite uptake by NMR. T-ALL $CD34^+/CD7^+$ cells were isolated from three T-ALL patients at presentation. The flow cytometry profile revealed that samples had cytoplasmic CD3 expression but lacked CD3 surface expression. T-ALL_1 had normal karyotype and consisted of 60% $CD34^+$ blasts, half of which were $CD7^+$. For T-ALL_2, karyotyping showed two lines of roughly equal proportion; normal 46XY and 47XY,add(1)(q3),add(7)(p1)x2,add(16)(q2),+21 and immunophenotypically was predominantly $CD7^+$, as well as $CD5^+$, $CD2^+$, $CD38^+$ and $CD4^+$. The T-ALL_3 karyotype was 46 XY-,t(10;14) with a trisomy 21 subclone and cells were $CD7^+$, $CD13^+$, $CD5^{+/-}$, $CD2^{+/-}$, $CD117^{+/-}$, while $CD1a^-$, $CD4^-$ and $CD8^-$. $CD34^+$ (T-ALL_1) or $CD7^+$ (T-ALL_2/3) cells were isolated and 10^6 cells were resuspended in RPMI medium supplemented with GlutaMAX (L-glutamine/L-alanine dipeptide) and used for measuring metabolite uptake.[30] GlutaMAX is a temperature-stable source of glutamine, which is hydrolyzed by peptidases located on the plasma membrane, into L-glutamine and L-alanine.[31] Using live-cell NMR we observed for all the patient samples that GlutaMAX concentrations decreased without the equivalent increase in glutamine availability showing that patient-derived T-ALL utilize glutamine (Figure 5A).

T-cell acute lymphoblastic leukemia cells express EAAT1 in the mitochondria

Our finding that T-ALL rely on deriving their aspartate from glutamine highlights that this metabolic step is a T-ALL liability. Therefore, we focused on identifying potential therapeutic targets for T-ALL treatment within the metabolic processes supporting glutamine-derived aspartate synthesis. Inhibiting the glutamate-aspartate anti-port across the mitochondrial membrane would be a good strategy for targeting T-ALL as it is not directed towards the enzymatic conversions that would restrict aspartate availability for nucleotide synthesis in healthy cells. Aspartate export and glutamate import into mitochondria is known to be facilitated by three different antiporters *SLC1A3*, *SLC25A12* and *SLC25A13*.[32,33] While *SLC25A12* and *SLC25A13* are expressed in most tissues, the expression of *SLC1A3* is mainly restricted to the CNS.[19,34] Published gene expression data of 264 T-ALL patient samples revealed that *SLC1A3* is expressed at various levels in 95% of patient samples (Figure 5B).[2] Further analysis of the patient samples showed that higher SLC1A3 expression correlated with the LMO1/2 and TAL1/2 subgroups (*Online Supplementary Figure S5*). There also seemed to be higher *SLC1A3* expression associated with an ETP or near ETP status, as defined by Liu *et al.*, although this was not statistically significant due to the low number of patients in these two groups. The presence of Notch mutations did not significantly correlate with *SLC1A3* expression levels.

Analysis of our RNAseq data showed *SLC1A3* expression in three of the T-ALL cell lines and an absence in T-cell progenitors, with subsequent quantitative polymerase chain reaction (qPCR) and western blotting confirming the expression of *SLC1A3* mRNA and EAAT1 protein (encoded by *SLC1A3*), in all four T-ALL cell lines (Figure 5C, D). We observed that EAAT1 was detected in the mitochondria of the T-ALL cell lines but not in the acute myeloid leukemia (AML) cell line Kasumi-1, which does not express *SLC1A3* (Figure 5C-E).[35] *SLC1A3* expression was not observed in mature $CD4^+$ or $CD8^+$ T cells, regardless of whether cells were stimulated (Figure 5F). For a direct comparison of *SLC1A3* expression between T-ALL patient samples and T-cell progenitors isolated from healthy thymus, we combined and analyzed published RNAseq data from ten different thymocyte populations[36] and 60 T-ALL patients.[37] These data sets were generated using the same platform at similar sequencing depth and were analyzed together. The results showed that significant SLC1A3 expression only occurred in T-ALL samples (*Online Supplementary Figure S6A*). Higher expression was particularly found in the TAL oncogenic subgroup (*Online Supplementary Figure S6B*) and less frequently in the immature, HoxA, and TLX3 subgroups, in line with the above findings (*Online Supplementary Figure S5*).

Together, these results show that T-ALL cells aberrantly overexpress the high affinity glutamate-aspartate anti-porter EAAT1.

SLC1A3/EAAT1 is essential for oncogenic *de novo* nucleotide synthesis

In order to assess the importance of EAAT1 for T-ALL survival we performed *SLC1A3* knock-down using shRNA. Five shSLC1A3 were designed and tested for their capacity to suppress the expression of *SLC1A3* cDNA. Mouse fibroblasts were co-transduced with retrovirus expressing SLC1A3-IRES-GFP and shRNA. shSLC1A3 efficiency was measured relative to the negative control, shFF3, and the positive control shGFP. shSLC1A3_1 and shSLC1A3_2 had the capacity to suppress EAAT1 protein levels similar to shGFP, while the negative control shFF3 did not have any effect on EAAT1 protein levels (Figure 6A). shSLC1A3_1 and shSLC1A3_2 were cloned into a PiggyBac backbone that supports stable doxycycline-inducible shRNA expression. Induction of shSLC1A3 led to rapid cell death within 5 days from the start of the doxycycline treatment (Figure 6B; *Online Supplementary Figure S7*).

A

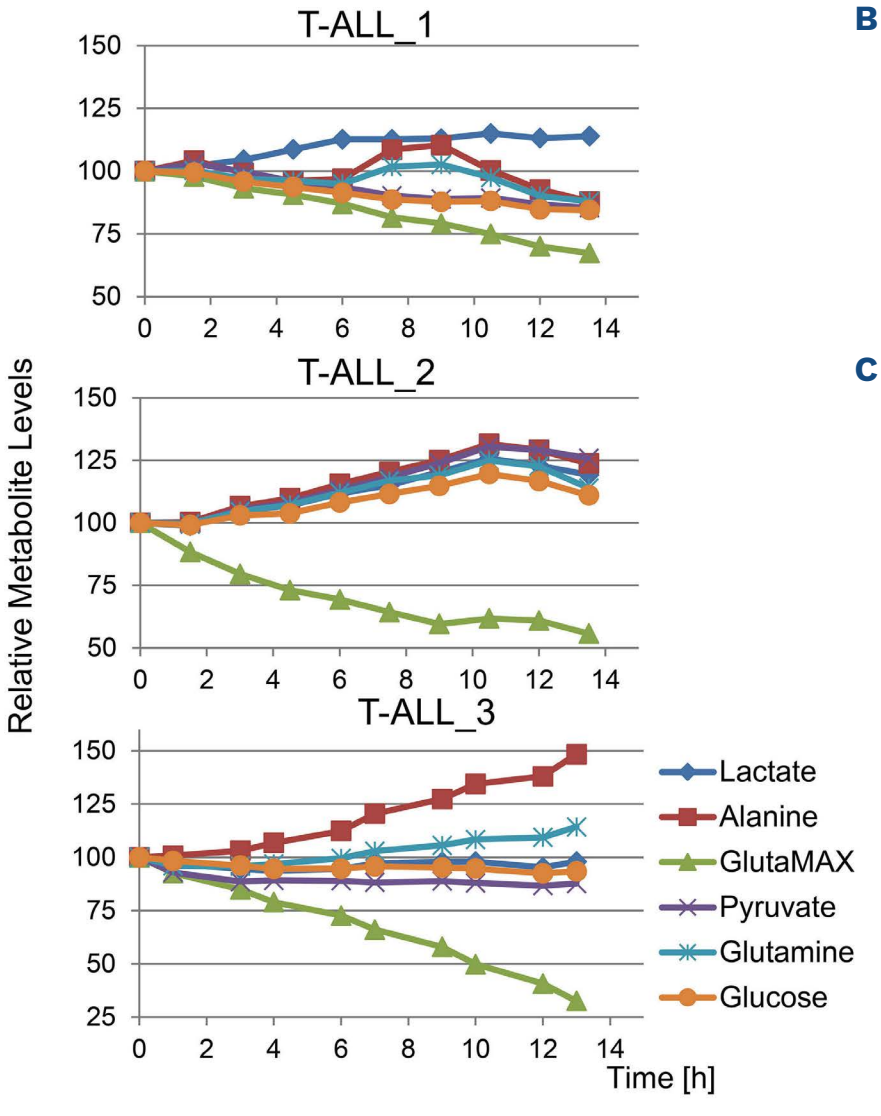

B

SLC1A3 mRNA levels in T-ALL patients

FPKM	0	Low [<0.1]	Medium [0.1-1]	High [1-40]
No of T-ALL	9	133	85	37

C

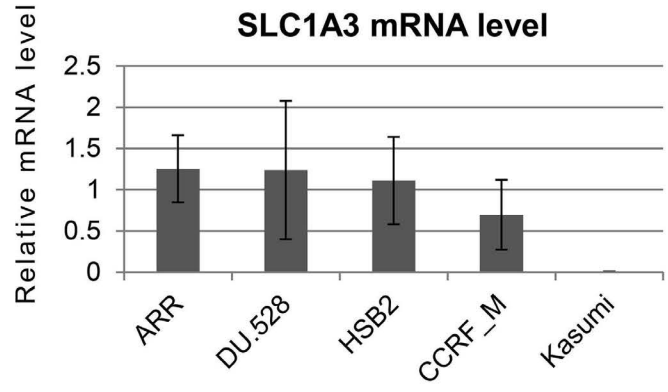

D

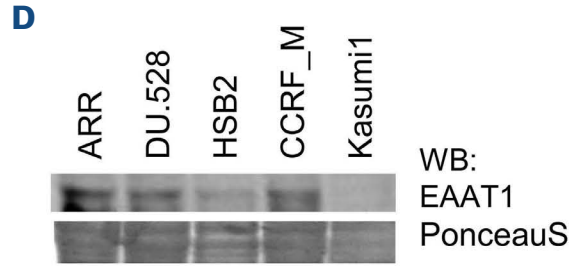

E

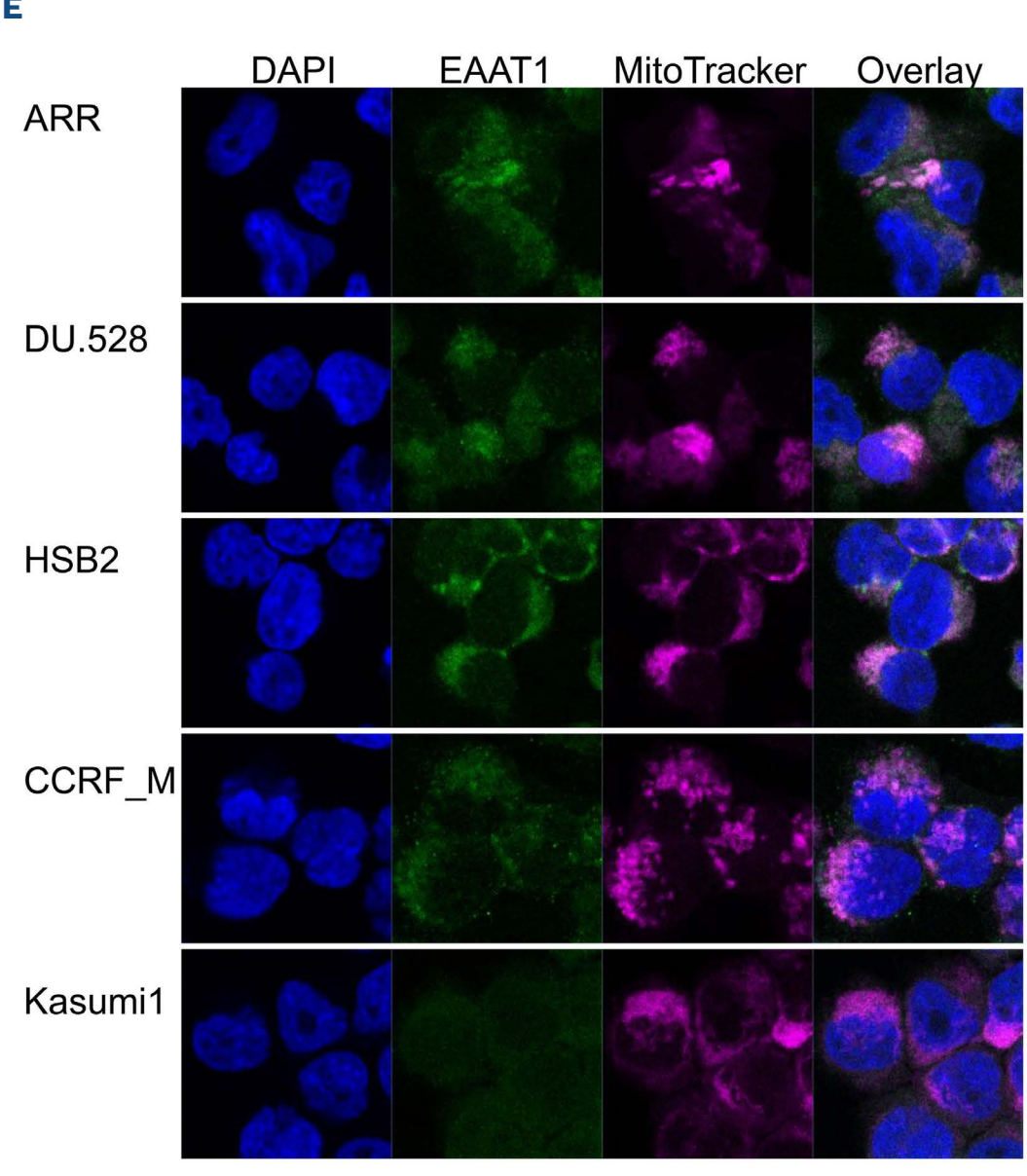

F

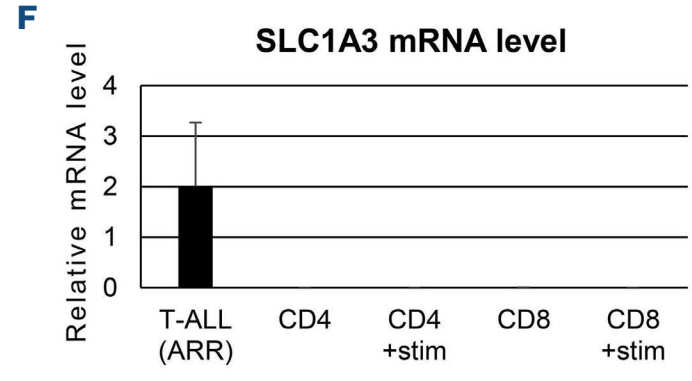

Continued on following page.

Figure 5. EAAT1 is expressed in T-cell acute lymphoblastic leukemia and localized in mitochondria. (A) Patient-derived T-cell acute lymphoblastic leukemia (T-ALL) cells have similar metabolic uptake to T-ALL cell lines. Only metabolites with changing concentration are illustrated. (B) Summary of the *SLC1A3* expression levels as assessed by FPKM values from the RNA sequencing of 265 patient samples. Data are grouped by the level of expression. (C) *SLC1A3* mRNA expression level in T-ALL cell lines and acute myeloid leukemia (AML) cell line Kasumi-1, relative to rRNA level assessed by quantitative polymerase chain reaction. (D) Western blot analysis of EAAT1 protein level using 150 μg total cell extract. PonceauS shows equal loading. (E) *SLC1A3* mRNA expression level in ARR and in unstimulated or stimulated $CD4^+$ or $CD8^+$ human T cells, relative to rRNA expression. $CD4^+$ and $CD8^+$ thymocytes data represent the average ± standard deviation of 6 independent samples. (F) Immuno-fluorescent imaging shows that EAAT1 (green) co-localizes with MitoTracker Red CMXRos (magenta) in T-ALL but not Kasumi-1. Magnification 250X.

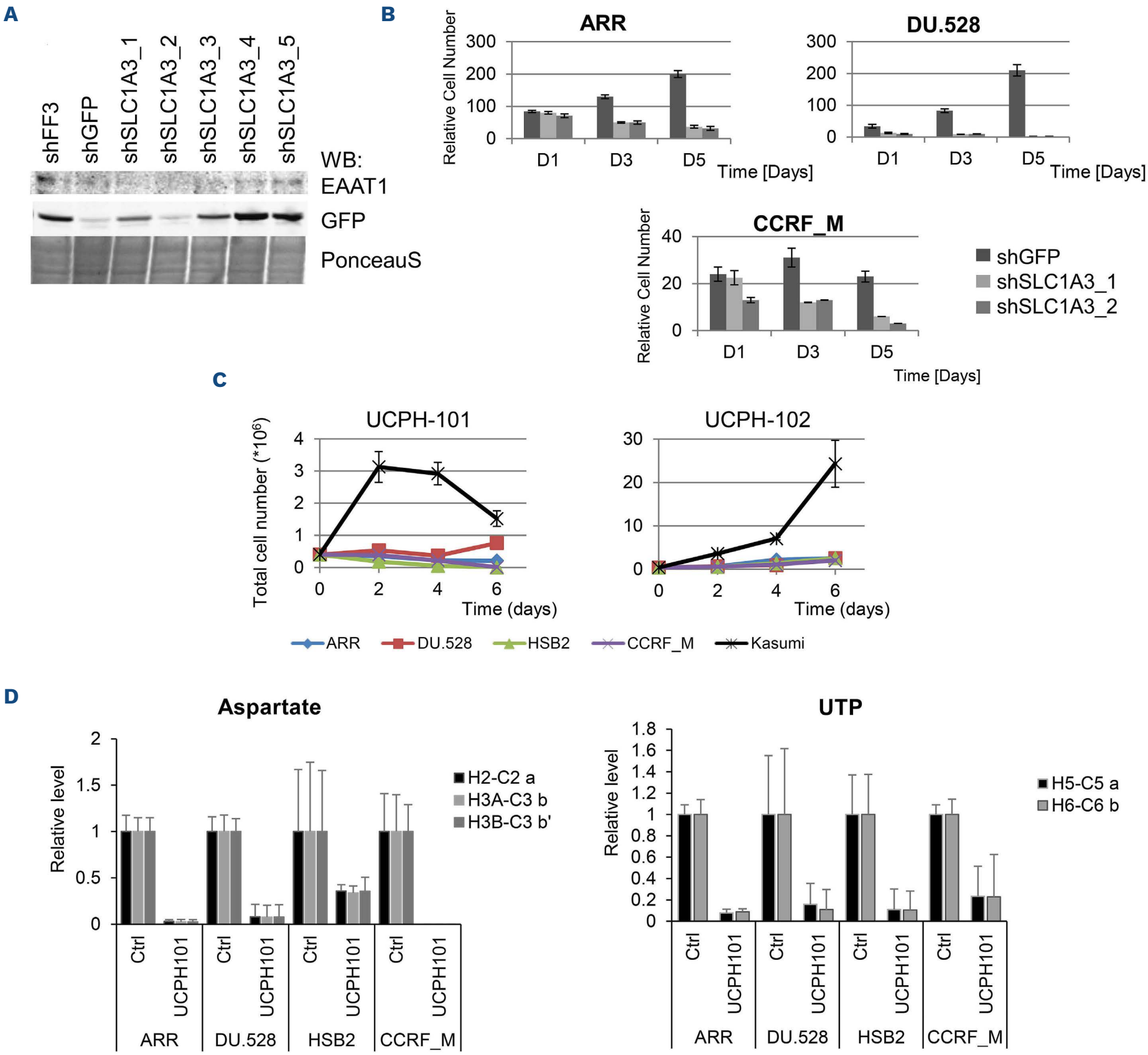

Figure 6. EAAT1 is essential for T-cell acute lymphoblastic leukemia proliferation and survival. (A) Protein level of EAAT1 and the reporter GFP protein upon the suppression of SLC1A3-IRES-GFP mRNA by short hairpin (sh)FF3 (negative control), shGFP (positive control) and 5 different shSLC1A3_1-5. Experiment was performed in duplicate. PonceauS staining illustrates equal loading. (B) Knock-down of the *SLC1A3* gene by shSLC1A3_1 and shSLC1A3_2 leads to ARR, DU.528 and CCRF_M cell death. (C) To test the

Continued on following page.

effect of EAAT1 inhibition, T-cell acute lymphoblastic leukemia (T-ALL) and acute myeloid leukemia (AML) cells were cultured for 6 days in the presence of vehicle (dimethyl sulfoxide [DMSO]), 25 μM UCPH-101, or 25 μM UCPH-102. Each data point is an average of 3 independent measurements ± standard deviation. (D) EAAT1 inhibition leads to a loss of aspartate and UTP production from glutamine. T-ALL cells were grown for 24 hours in culture media containing [3-^{13}C]glutamine in the presence of 25 μM UCPH-101 or vehicle (DMSO). Bar graphs show ^{13}C signal intensity relative to the DMSO control. Each bar represents one of the interactions shown in the schematics in Figure 4A. Data are the average of 3 independent experiments ± standard deviation. UTP: uridine-5'-triphosphate.

With the purpose to inhibit EAAT1 function in the CNS, two specific allosteric inhibitors, UCPH-101 and UCPH-102 were developed.[38,39] Both drugs exhibited inhibitory effects on T-ALL proliferation (Figure 6C; *Online Supplementary Figure S8*). UCPH-101 also affected the growth and survival of the control AML cell line Kasumi-1 when cultured for more than 2 days, which can be explained by the presence of known toxophores. UCPH-102 had a specific anti-proliferative effect only on T-ALL cells. Next we performed [3-^{13}C]glutamine tracing experiments upon EAAT1 inhibition, which showed a marked decrease in the production of aspartate and UTP from glutamine (Figure 6D). Altogether, our results show that oncogenic nucleotide production depends on EAAT1 function and glutamine conversion to aspartate.

EAAT1 is required for T-cell acute lymphoblastic leukemia xenograft development

In order to test the importance of EAAT1 during disease progression in a mouse xenograft model, CRRF-CEM cells, carrying doxycycline-inducible shSLC1A3_2 or shGFP in conjunction with TdTomato, were injected into the tail vein of NSG mice. When engraftment was apparent at approximately 1% of total CD45$^+$ blood mononuclear cells, the diet was supplemented with doxycycline to induce shRNA expression. After 6 days, significantly less human CD45$^+$ cells were detected in mice with shSLC1A3-expressing CCRF-CEM cells, compared to mice that received shGFP-expressing cells (Figure 7A; *Online Supplementary Figure S9*). Doxycycline treatment resulted in a survival advantage for the shSLC1A3 mice compared to the shGFP control mice (Figure 7B). While all human CD45$^+$ shGFP-expressing cells

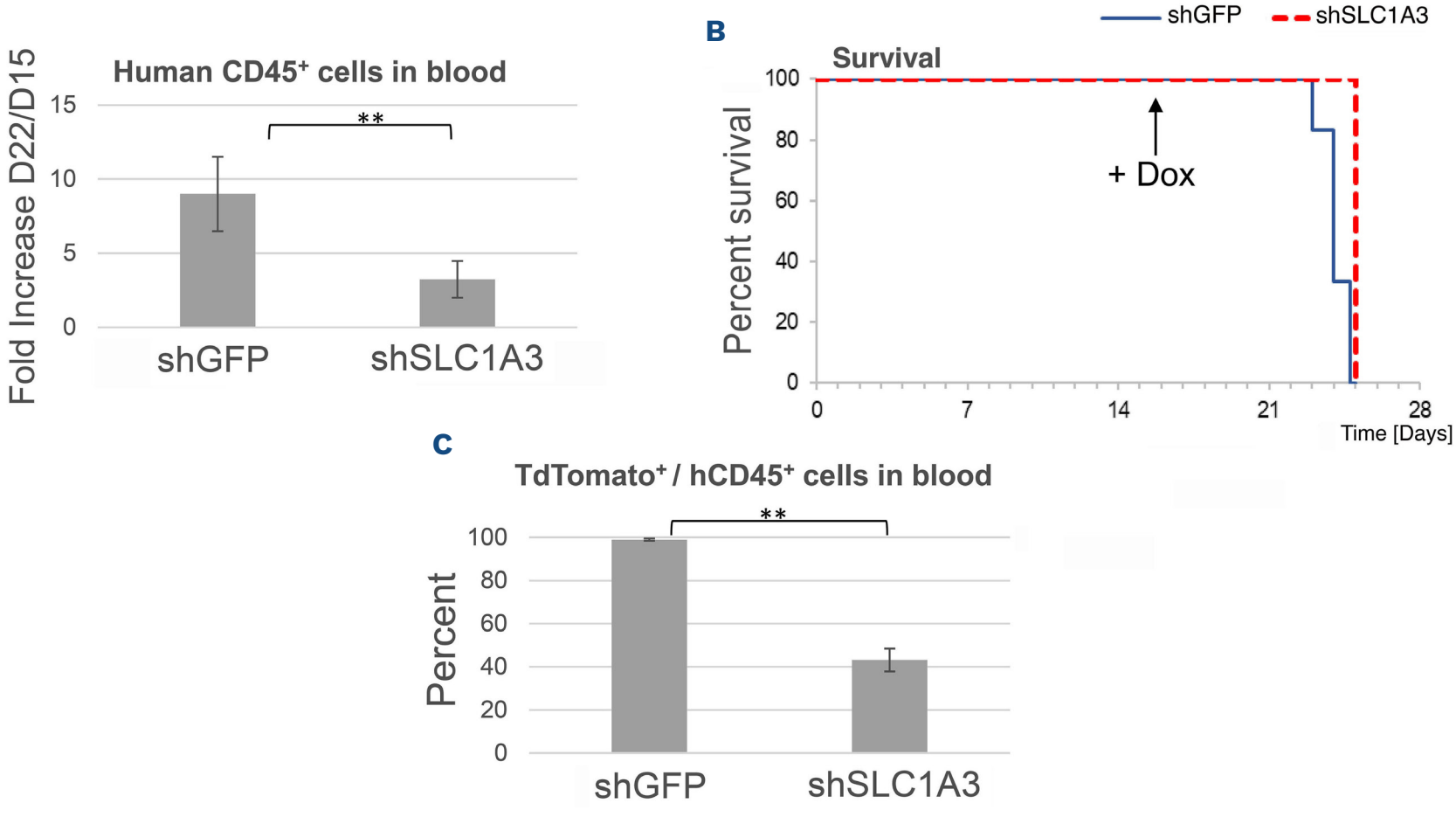

Figure 7. EAAT1 is required for T-cell acute lymphoblastic leukemia xenograft development. (A) Mice were injected (iv) with 3x10^5 CCRF-CEM cells carrying doxycycline-inducible short hairpin (sh)SLC1A3_2 or shGFP. At day 16, the food was supplemented with doxycycline. The bar graph shows the expansion of human CD45$^+$ cells in the 2 cohorts of mice (N=5) during 6 days of doxycycline treatment. Two-tailed *t* test identified the difference between the 2 cohorts as significantly different (P<0.01). (B) Kaplan- Meier curve comparing the survival of mice injected with CCRF-CEM cells carrying doxycycline-inducible shSLC1A3 or shGFP. The induction of shRNA expression through addition of doxycycline in the food on day 16 is indicated. Log-rank test (right-tailed) identified the difference between the 2 cohorts as significantly different (P<0.05). (C) The number of TdTomato-positive cells relative to the total number of hCD45$^+$ cells at day 6. Two-tailed *t* test identified the difference between the 2 cohorts as significantly different (P<0.01).

were TdTomato-positive, this was the case for only 40% of human CD45$^+$ cells in mice with shSLC1A3-expressing cells, indicating the outgrow of cells that did no longer express the shSLC1A3 construct (Figure 7C). These *in vivo* results show that EAAT1 gives a proliferative advantage to T-ALL and validates EAAT1 as therapeutic target.

Discussion

Understanding the metabolic pathways that support oncogenic proliferation can help to identify cancer-specific processes and rate-limiting steps that can be used for developing new therapies. We show that in T-ALL cells, glutamine is converted to glutamate that enters the mitochondria. Here, glutamate dehydrogenase (GLUD1,2) uses it to generate α-ketoglutarate that will enter the TCA cycle (Figure 8). Mitochondrial glutamate oxaloacetate transaminase (GOT2) uses glutamate as a donor for the amino group, which is transferred to the TCA cycle intermediate oxaloacetate, resulting in the generation of aspartate. Aspartate is then transported out of the mitochondria in exchange for a new glutamate molecule. Together, glutamine and aspartate are used as substrates for nucleotide synthesis (Figure 8).

Similar processes are likely to occur in other cancers. Indeed, a recent study of genetic cancer dependencies has shown that T-ALL and several other cancer types are dependent on *SLC1A3* expression.[40] Additionally, EAAT1 has been implicated in supporting proliferation in several solid cancer cell lines.[41,42] These studies showed a role for EAAT1 in the uptake of aspartate from the medium, especially under conditions of glutamine deprivation or asparaginase treatment. In both studies, removing EAAT1 under normal cell culture conditions showed little or no effect, in contrast to our work with T-ALL cells. This difference can be explained as the solid tumor cell lines were mainly dependent on EAAT1 for aspartate/glutamate uptake from the environment and the lack thereof resulted in a combinatorial effect on the TCA cycle, the electron transport chain, and *de novo* glutamine/glutamate and nucleotide synthesis. T-ALL cells on the other hand are dependent on the availability of glutamine. They rely on the function of EAAT1 at the mitochondria, where the glutamate/aspartate antiport is required for *de novo* nucleotide production. Our isotope tracing experiments show that the carbon and nitrogen atoms of glutamine are used for aspartate, purine and pyrimidine biosynthe-

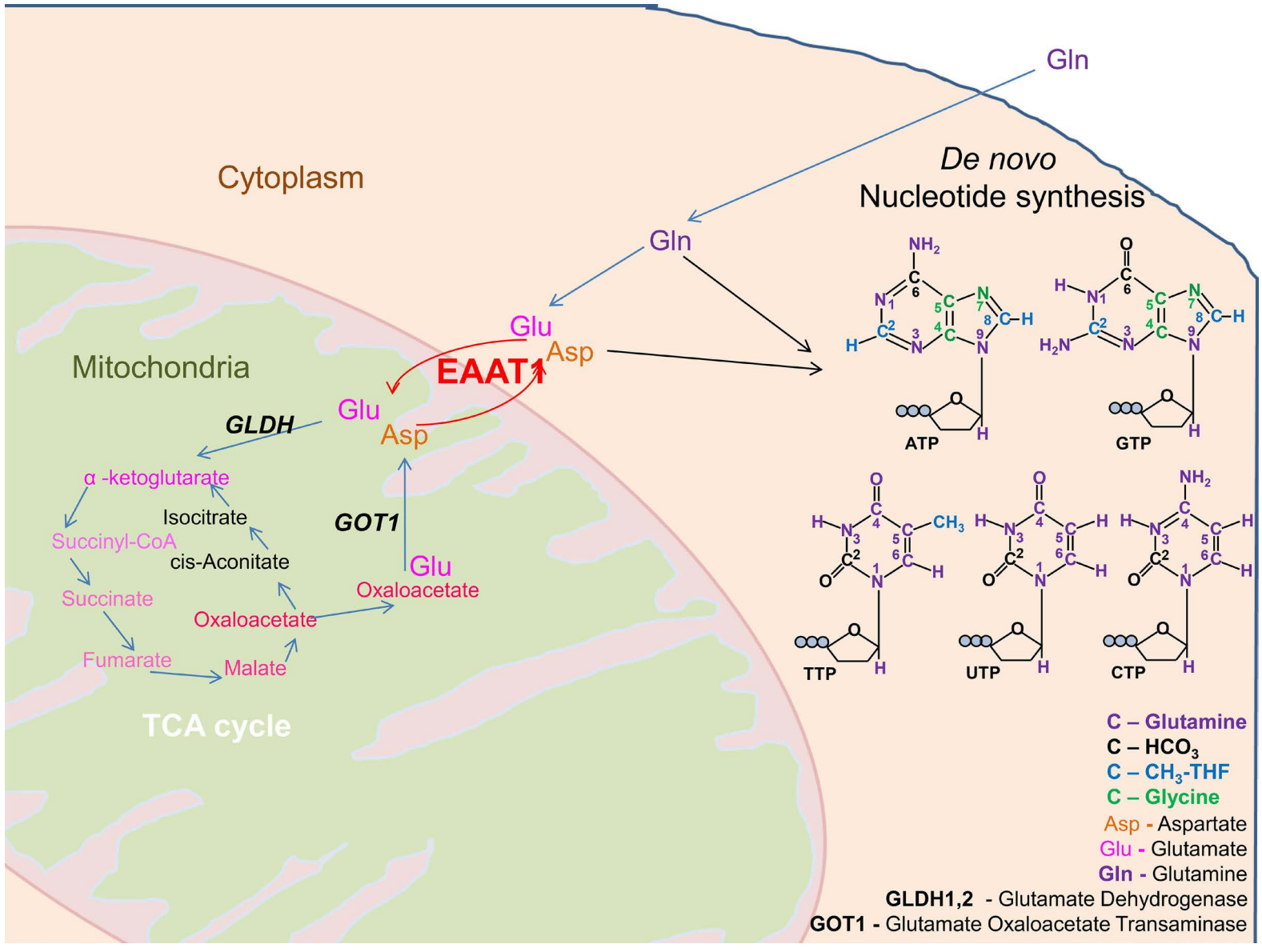

Figure 8. Model illustrating the function of mitochondrial EAAT1.

sis. Sun *et al*. also showed that asparaginase treatment resulted in a cellular depletion of glutamine/glutamate, possibly explaining why asparaginase treatment is often effective in treatment of T-ALL.[43]

EAAT1 is normally present on the plasma membrane of neurons and glia in the CNS, where it uptakes glutamate from the glutamatergic synapses.[18] Based on the RNA expression and protein localization assessed with three different specific antibodies, the Human Protein Atlas Database reports that EAAT1 is not found at significant levels outside of the CNS (https://www.proteinatlas.org/ENSG00000079215-SLC1A3/tissue).[44] However, EAAT1 expression has been reported in neonatal cardiomyocytes where, similar to T-ALL, it is also localized at the mitochondria. Here it is present together with two other glutamate-aspartate antiporters, *i.e*., ARALAR1 and CITRIN[32]. ARALAR1 and CITRIN are calcium-binding mitochondrial carrier proteins that import a glutamate molecule together with a H^+ into the mitochondria in exchange for the export of an aspartate anion.[45-47] Their activity depends on the mitochondrial membrane potential that is maintained by cytoplasmic ATP.[48] Both transporters are present in most cells and tissues (reviewed in [49]). We found that SLC25A12 (encoding ARALAR1) is expressed in all four T-ALL cell lines, while SLC25A13 (encoding CITRIN) was found only in DU.528. T-ALL cells likely rely on EAAT1 because intracellular conditions, such as the pH, ATP availability and mitochondrial action potential, are restrictive for ARALAR1 and CITRIN, whereas EAAT1 is independent of these factors. It is known that T-ALL is dependent on AMPK activity, indicating low ATP availability.[50] Consequently, EAAT1 might also be important for maintaining mitochondrial potential when ATP availability is reduced.

Altogether, we show that *SLC1A3* is aberrantly expressed in T-ALL cells, where it supports *de novo* nucleotide production which uses glutamine as the main substrate, and that EAAT1 is required for T-ALL proliferation, identifying it as a relevant therapeutic target. Unfortunately, the selective and potent EAAT1 inhibitor UCPH-102, which has been developed for the inhibition of EAAT1 in the CNS, is not suitable for *in vivo* use and therefore new therapeutic agents need to be developed that can target the oncogenic function of EAAT1.

Disclosures

No conflicts of interest to disclose.

Contributions

Project planning and experimental design by VSS and MH. NMR data acquisition and analysis by VSS, MACR, JR, UG and CL. Animal experiments by VSS, TAP and MH. Other experimentation, data acquisition, processing and analyses by VSS, SAO, ELB, TF-W, NG, JR, TT and MH. Statistical analysis by VSS, JR and MH. Provision of patient samples by SP and GP. Provision of reagents by SS and SD. Design of figures by VSS, JR, CL and MH. Writing of the manuscript by VSS and MH.

Acknowledgments

We would like to thank Dr. A.W. Langerak, (Erasmus Medical Center, Rotterdam, NL) for the provision of ARR and DU.528 cell lines and Prof P.N. Cockerill (University of Birmingham, UK) for HSB2 and CCRF-CEM. We would like to thank Dr. M. McGrew (University of Edinburgh, UK) for the PB_tet-on_Apple_shGFP plasmid and Prof. L. Bunch (University of Copenhagen, Denmark) for pcDNA3-EAAT1 plasmid. We would like to acknowledge the University of Birmingham FACS facility for cell sorting and the Biomolecular NMR Facility at the Henry Wellcome Building for Nuclear Magnetic Resonance (HWB-NMR), University of Birmingham. We gratefully acknowledge the contribution to this study made by the University of Birmingham's Human Biomaterials Resource Center, which was set up with support from the Birmingham Science City - Experimental Medicine Network of Excellence project.

Funding

This work was supported by Blood Cancer UK, through a Bennett Fellowship to MH (11002).

Data-sharing statement

T-ALL RNAseq data is available at NCBI-GEO GSE101566.

References

1. Homminga I, Pieters R, Langerak AW, et al. Integrated transcript and genome analyses reveal NKX2-1 and MEF2C as potential oncogenes in T cell acute lymphoblastic leukemia. Cancer Cell. 2011;19(4):484-497.
2. Liu Y, Easton J, Shao Y, et al. The genomic landscape of pediatric and young adult T-lineage acute lymphoblastic leukemia. Nat Genet. 2017;49(8):1211-1218.
3. Chessells JM, Veys P, Kempski H, et al. Long-term follow-up of relapsed childhood acute lymphoblastic leukaemia. Br J Haematol. 2003;123(3):396-405.
4. Vora A, Wade R, Mitchell CD, Goulden N, Richards S. Improved outcome for children and young adults with T-cell acute lymphoblastic leukaemia (ALL): results of the United Kingdom Medical Research Council (MRC) Trial UKALL 2003. Blood. 2008; 112(11):908.
5. Hastings C, Gaynon PS, Nachman JB, et al. Increased post-induction intensification improves outcome in children and adolescents with a markedly elevated white blood cell count (>/=200 x 10(9) /l) with T cell acute lymphoblastic leukaemia but not B cell disease: a report from the Children's Oncology Group. Br J Haematol. 2015;168(4):533-546.
6. Vora A, Goulden N, Mitchell C, et al. Augmented post-remission

therapy for a minimal residual disease-defined high-risk subgroup of children and young people with clinical standard-risk and intermediate-risk acute lymphoblastic leukaemia (UKALL 2003): a randomised controlled trial. Lancet Oncol. 2014;15(8):809-818.
7. Nagarajan A, Malvi P, Wajapeyee N. Oncogene-directed alterations in cancer cell metabolism. Trends Cancer. 2016;2(7):365-377.
8. Shoshan M. On mitochondrial metabolism in tumor biology. Curr Opin Oncol. 2017;29(1):48-54.
9. Tennant DA, Duran RV, Gottlieb E. Targeting metabolic transformation for cancer therapy. Nat Rev Cancer. 2010;10(4):267-277.
10. Mossmann D, Park S, Hall MN. mTOR signalling and cellular metabolism are mutual determinants in cancer. Nat Rev Cancer. 2018;18(12):744-757.
11. Fruman DA, Rommel C. PI3K and cancer: lessons, challenges and opportunities. Nat Rev Drug Discov. 2014;13(2):140-156.
12. Mayer IA, Arteaga CL. The PI3K/AKT pathway as a target for cancer treatment. Annu Rev Med. 2016;67:11-28.
13. Raivio KO, Andersson LC. Glutamine requirements for purine metabolism in leukemic lymphoblasts. Leuk Res. 1982;6(1):111-115.
14. Kitoh T, Kubota M, Takimoto T, et al. Metabolic basis for differential glutamine requirements of human leukemia cell lines. J Cell Physiol. 1990;143(1):150-153.
15. Hu J, Wang T, Xu J, et al. WEE1 inhibition induces glutamine addiction in T-cell acute lymphoblastic leukemia. Haematologica. 2021;106(7):1816-1827.
16. Herranz D, Ambesi-Impiombato A, Sudderth J, et al. Metabolic reprogramming induces resistance to anti-NOTCH1 therapies in T cell acute lymphoblastic leukemia. Nat Med. 2015;21(10):1182-1189.
17. Nguyen TL, Nokin MJ, Teres S, et al. Downregulation of glutamine synthetase, not glutaminolysis, is responsible for glutamine addiction in Notch1-driven acute lymphoblastic leukemia. Mol Oncol. 2021;15(5):1412-1431.
18. Lehre KP, Levy LM, Ottersen OP, Storm-Mathisen J, Danbolt NC. Differential expression of two glial glutamate transporters in the rat brain: quantitative and immunocytochemical observations. J Neurosci. 1995;15(3 Pt 1):1835-1853.
19. Storck T, Schulte S, Hofmann K, Stoffel W. Structure, expression, and functional analysis of a Na(+)-dependent glutamate/aspartate transporter from rat brain. Proc Natl Acad Sci U S A. 1992;89(22):10955-10959.
20. Stanulovic VS, Cauchy P, Assi SA, Hoogenkamp M. LMO2 is required for TAL1 DNA binding activity and initiation of definitive haematopoiesis at the haemangioblast stage. Nucleic Acids Res. 2017;45(17):9874-9888.
21. Pear WS, Miller JP, Xu L, et al. Efficient and rapid induction of a chronic myelogenous leukemia-like myeloproliferative disease in mice receiving P210 bcr/abl-transduced bone marrow. Blood. 1998;92(10):3780-3792.
22. Dow LE, Premsrirut PK, Zuber J, et al. A pipeline for the generation of shRNA transgenic mice. Nat Protoc. 2012;7(2):374-393.
23. Morita S, Kojima T, Kitamura T. Plat-E: an efficient and stable system for transient packaging of retroviruses. Gene Ther. 2000;7(12):1063-1066.
24. Paddison PJ, Cleary M, Silva JM, et al. Cloning of short hairpin RNAs for gene knockdown in mammalian cells. Nat Methods. 2004;1(2):163-167.
25. Glover JD, Taylor L, Sherman A, Zeiger-Poli C, Sang HM, McGrew MJ. A novel piggyBac transposon inducible expression system identifies a role for AKT signalling in primordial germ cell migration. PLoS One. 2013;8(11):e77222.
26. Wang W, Lin C, Lu D, et al. Chromosomal transposition of PiggyBac in mouse embryonic stem cells. Proc Natl Acad Sci U S A. 2008;105(27):9290-9295.
27. Ludwig C, Gunther UL. MetaboLab--advanced NMR data processing and analysis for metabolomics. BMC Bioinformatics. 2011;12:366.
28. Sandberg Y, Verhaaf B, van Gastel-Mol EJ, et al. Human T-cell lines with well-defined T-cell receptor gene rearrangements as controls for the BIOMED-2 multiplex polymerase chain reaction tubes. Leukemia. 2007;21(2):230-237.
29. Etchin J, Sanda T, Mansour MR, et al. KPT-330 inhibitor of CRM1 (XPO1)-mediated nuclear export has selective anti-leukaemic activity in preclinical models of T-cell acute lymphoblastic leukaemia and acute myeloid leukaemia. Br J Haematol. 2013;161(1):117-127.
30. Roth E, Ollenschlager G, Hamilton G, et al. Influence of two glutamine-containing dipeptides on growth of mammalian cells. In Vitro Cell Dev Biol. 1988;24(7):696-698.
31. Christie A, Butler M. Glutamine-based dipeptides are utilized in mammalian cell culture by extracellular hydrolysis catalyzed by a specific peptidase. J Biotechnol. 1994;37(3):277-290.
32. Ralphe JC, Segar JL, Schutte BC, Scholz TD. Localization and function of the brain excitatory amino acid transporter type 1 in cardiac mitochondria. J Mol Cell Cardiol. 2004;37(1):33-41.
33. Lasorsa FM, Pinton P, Palmieri L, Fiermonte G, Rizzuto R, Palmieri F. Recombinant expression of the Ca(2+)-sensitive aspartate/glutamate carrier increases mitochondrial ATP production in agonist-stimulated Chinese hamster ovary cells. J Biol Chem. 2003;278(40):38686-38692.
34. Fagerberg L, Hallstrom BM, Oksvold P, et al. Analysis of the human tissue-specific expression by genome-wide integration of transcriptomics and antibody-based proteomics. Mol Cell Proteomics. 2014;13(2):397-406.
35. Ptasinska A, Assi SA, Martinez-Soria N, et al. Identification of a dynamic core transcriptional network in t(8;21) AML that regulates differentiation block and self-renewal. Cell Rep. 2014;8(6):1974-1988.
36. Roels J, Kuchmiy A, De Decker M, et al. Distinct and temporary-restricted epigenetic mechanisms regulate human alphabeta and gammadelta T cell development. Nat Immunol. 2020;21(10):1280-1292.
37. Verboom K, Van Loocke W, Volders PJ, et al. A comprehensive inventory of TLX1 controlled long non-coding RNAs in T-cell acute lymphoblastic leukemia through polyA+ and total RNA sequencing. Haematologica. 2018;103(12):e585-e589.
38. Erichsen MN, Huynh TH, Abrahamsen B, et al. Structure-activity relationship study of first selective inhibitor of excitatory amino acid transporter subtype 1: 2-amino-4-(4-methoxyphenyl)-7-(naphthalen-1-yl)-5-oxo-5,6,7,8-tetrahydro-4H-chrom ene-3-carbonitrile (UCPH-101). J Med Chem. 2010;53(19):7180-7191.
39. Canul-Tec JC, Assal R, Cirri E, et al. Structure and allosteric inhibition of excitatory amino acid transporter 1. Nature. 2017;544(7651):446-451.
40. Tsherniak A, Vazquez F, Montgomery PG, et al. Defining a cancer dependency map. Cell. 2017;170(3):564-576.
41. Sun J, Nagel R, Zaal EA, et al. SLC1A3 contributes to L-asparaginase resistance in solid tumors. EMBO J. 2019;38(21):e102147.

42. Tajan M, Hock AK, Blagih J, et al. A role for p53 in the adaptation to glutamine starvation through the expression of SLC1A3. Cell Metab. 2018;28(5):721-736.
43. Pui CH, Campana D, Pei D, et al. Treating childhood acute lymphoblastic leukemia without cranial irradiation. N Engl J Med. 2009;360(26):2730-2741.
44. Uhlen M, Fagerberg L, Hallstrom BM, et al. Proteomics. Tissue-based map of the human proteome. Science. 2015;347(6220):1260419.
45. Thangaratnarajah C, Ruprecht JJ, Kunji ER. Calcium-induced conformational changes of the regulatory domain of human mitochondrial aspartate/glutamate carriers. Nat Commun. 2014;5:5491.
46. Palmieri L, Pardo B, Lasorsa FM, et al. Citrin and aralar1 are Ca(2+)-stimulated aspartate/glutamate transporters in mitochondria. EMBO J. 2001;20(18):5060-5069.
47. LaNoue KF, Tischler ME. Electrogenic characteristics of the mitochondrial glutamate-aspartate antiporter. J Biol Chem. 1974;249(23):7522-7528.
48. LaNoue KF, Bryla J, Bassett DJ. Energy-driven aspartate efflux from heart and liver mitochondria. J Biol Chem. 1974;249(23):7514-7521.
49. Amoedo ND, Punzi G, Obre E, et al. AGC1/2, the mitochondrial aspartate-glutamate carriers. Biochim Biophys Acta. 2016;1863(10):2394-2412.
50. Kishton RJ, Barnes CE, Nichols AG, et al. AMPK Is Essential to balance glycolysis and mitochondrial metabolism to control T-ALL cell stress and survival. Cell Metab. 2016;23(4):649-662.